J Mol Model (2012) 18:3669–3694
DOI 10.1007/s00894-012-1363-x

ORIGINAL PAPER

3D-QSAR study of Chk1 kinase inhibitors based on docking

Lingzhou Zhao · Yongjuan Liu · Shiyuan Hu · Huabei Zhang

Received: 21 October 2011 / Accepted: 17 January 2012 / Published online: 25 February 2012

Abstract Checkpoint kinase 1 (Chk1), a kind of a serine/threonine protein kinase, plays a significant role in DNA damage-induced checkpoints. Chk1 inhibitors have been demonstrated to abrogate the S and G2 checkpoints and disrupt the DNA repair process, which results in immature mitotic progression, mitotic catastrophe, and cell death. Normal cells remain at the G1 phase via p53 to repair their DNA damages, and are less influenced by the abrogation of S and G2 checkpoint. Therefore, selective inhibitors of Chk1 may be of great therapeutic value in cancer treatment. In this paper, in order to understand the structure-activity relationship of macro-cyclic urea Chk1 inhibitors, a study combined molecular docking and 3D-QSAR modeling was carried out, which resulted in two substructure-based 3D-QSAR models, including the CoMFA model (r^2, 0.873; q^2, 0.572) and CoMSIA model (r^2, 0.897; q^2, 0.599). The detailed microscopic structures of Chk1 binding with inhibitors were performed by molecular docking. Two docking based 3D-QSAR models were developed (CoMFA with r^2, 0.887; q^2, 0.501; CoMSIA with r^2, 0.872; q^2, 0.520). The contour maps obtained from the 3D-QSAR models in combination with the docked binding structures would be helpful to better understand the structure–activity relationship. All the conclusions drawn from both the 3D-QSAR contour maps and molecular docking were in accordance with the experimental activity dates. The results suggested that the developed models and the obtained CHk1 inhibitor binding structures might be reliable to predict the activity of new inhibitors and reasonable for the future drug design.

L. Zhao · Y. Liu · S. Hu · H. Zhang (✉)
Key Laboratory of Radiopharmaceuticals of Ministry of Education, College of Chemistry, Beijing Normal University, Beijing 100875, China
e-mail: hbzhang@bnu.edu.cn

Keywords CHK1·docking · CoMFA · CoMSIA · 3D-QSAR

Introduction

It is important for living organisms to accurately transmit genetic materials to their offspring. However, they will face many challenges, including the inevitable errors during the normal DNA replication and the DNA damages caused by the endogenous (e.g. metabolites) or exogenous genotoxic substances (such as ultraviolet light and ionizing radiation). If the DNA damage cannot be repaired, the accurately transmitting genetic information will be uncompleted. In order to retain genomic integrity, some mechanisms have evolved in cells, such as checkpoints which detect genomic defects and start a response to deal with them by a complicated network of signal transduction pathways consisting of sensors, transducers, and effectors. Sensors inspect DNA damage and abnormal DNA structures, and then send out signals that are magnified by transducers and transmitted to effectors; effectors could carry out various activities including stopping cell cycle transitions and repairing damaged DNA as well as cell death [1].

In the past few decades, there have been many reports about Chk1 as a conservative protein kinase in process of biological evolution and could regulate the cell cycle progression in the S and G2/M checkpoint. When ionizing radiation, ultraviolet radiation or other factors induce DNA damage or the stagnation of DNA replication, the Chk1 is activated. The activated Chk1 could stimulate cells to produce the cell cycle block, DNA repair or cell apoptosis [2–4], which plays a very important role in the regulation of cell cycle checkpoints caused by the DNA damage. The steady expression of Chk1 kinase protein is conducive to the maintenance of repairing DNA damage and regulating cell

cycle checkpoint, to ensure the integrity and stability of the cell genome [5]. Human Chk1 is a nuclear protein of 476 amino acids, containing a highly conserved N-terminal kinase domain (residues1-265), a flexible linker region, SQ/TQ region and a less-conserved C-terminal region which may negatively regulate Chk1 kinase activity. Tumor cells with Chk1 deficiency showed multiple defects: slow cell proliferation, disappearance of cell cycle checkpoints response, and increased sensitivity to DAN damaging agents. Chk1 as a new tumor cell target for radiation and chemotherapy treatment to increase susceptibility effect has drawn wide public concern to the academic and pharmaceutical industry. Currently, many labs have carried out a variety of important research on the Chk1 kinase inhibitors. Especially, Abbott Laboratories have developed several basic skeletons of the Chk1 inhibitors. One of these basic skeletons, macro-cyclic urea, has been selected to perform molecular docking and 3D-QSAR research in this paper.

Compared with traditional QSAR models derived from molecular descriptors, 3D-QSAR models could give more information about the influence of the agonist conformation on the activity which would be useful for the further structural modification. In addition, combining with docking study, 3D-QSAR could provide more information on the interaction mode between the inhibitor and the receptor. Ligand- and receptor-based 3D-QSAR approaches have been proved to be valuable in further optimization and the development of novel inhibitors. In this paper, 3D-QSAR studies were performed for the Chk1 by using comparative molecular field analysis (CoMFA) [6, 7] and comparative molecular similarity analysis (CoMSIA) [8] with molecular docking approach to predict the biological activity of new compounds. Besides, some beneficial information was provided in structural modifications for designing new agonists with desired binding affinities with Chk1. In CoMFA, steric and electrostatic interaction energies of molecules were correlated with their biological activity [9]. In CoMSIA, additional molecular descriptors such as hydrophobic fields, hydrogen-bond donor and acceptor fields were included, and similarity indices were calculated at regularly placed grid points for the aligned molecules. Both 3D-QSAR methods provided contour maps as output that could be used to get some general insights into the topological features of the binding site [10].

In conventional ligand-based QSAR, the active conformations are obtained through minimizing the molecules and selecting those with lower energy. While receptor-based conformations are determinate by docking and take into account features of the binding pocket. Thus the derived models are more credible. The binding conformations of these antagonists and their alignment in the active site of the receptor are used to build 3D-QSAR models, which could be further applied in activity prediction at a faster speed [11].

Computational details

Data sets and alignment

In this report, a total of 174 Chk1 kinase inhibitors were collected from the same lab Abbott Laboratories [12–17]. The 174 compounds shown in Table 1 were randomly divided into training set and test set comprised of 140 and 34 molecules respectively. The training set was used to construct 3D-QSAR models and the test set was used for the models validation. The test-set compounds had a range of biological activity values similar to that of the training set. To derive the CoMFA and CoMSIA models, all the activity values of the CHK1 inhibitor reported as IC_{50} in the literature were converted to pIC_{50} ($-\log IC_{50}$) and used as dependent variables in the CoMFA and CoMSIA calculations. Molecular structures and their pIC_{50} values were presented in Table 1. The pIC_{50} values were from 5.86 to 9.52, covering 4 log units. A/Q77A1001 inhibitor had been selected as a template (Fig. 1) [18]. The X-ray crystal structure 2E9P was selected from the Protein Data Bank (PDB, http://www.rcsb.org/pdb) (Fig. 2), and X crystal diffraction resolution was 2.60 Å.

Molecular modeling

The entire molecular model and its calculations were generated using Sybyl 7.0 molecular modeling package [19] on a Silicon Graphics O2 workstation, running under RHEL 4 Operating System. The chemical structures of the model were constructed under the package of Sketch Molecule, included in Sybyl Software. Energy minimizations were performed using the Tripos force field with a distance-dependent dielectric and conjugated gradient algorithm with a convergence criterion of 0.005 kcal/ mol [20] and their partial atomic charges were calculated using Gasteiger–Hückel method [21]. The partial atomic charges required for electrostatic interaction were computed by semi-empirical molecular orbital methods using MOPAC with AM1 Hamiltonian (with key word “MMOK” in the process). The common structure built on the A/Q77A1001 in Fig. 3, and the alignment containing test set and training set have been displayed in Fig. 4, generated in database alignment in Sybyl.

Generation of CoMFA and CoMSIA models

CoMFA and CoMSIA analyses were conducted on the optimal binding conformations using conformational searching module and their alignments originated from docking calculation, to build predictive QSAR models and to estimate the contributions of steric, electrostatic, hydrophobic, hydrogen donor and acceptor effects to the activities

Table 1 Chemical structure of inhibitors and their activities for Chk1

Structure A	**No**	**R**	IC_{50}(nM)	**PIC_{50}**
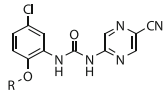	***A001**	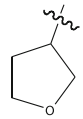	3	8.52
	A002	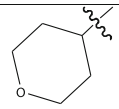	5	8.30
	A003	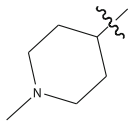	10	8.00
	A004	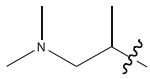	8	8.10
	A005	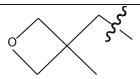	7	8.15
Structure B	**No**	**R^4**	IC_{50}(nM)	**PIC_{50}**
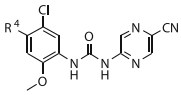	***B006**	CH_3O	7	8.15
	B007	$-NO_2$	42	7.38
	B008	$-NH_2$	5	8.30
	B009	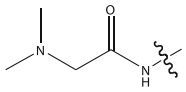	3	8.52
	B010	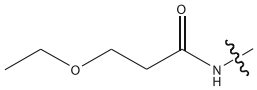	22	7.66
	***B011**	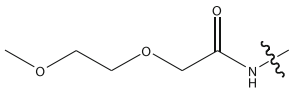	18	7.74
	B012	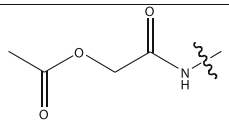	9	8.05
	B013	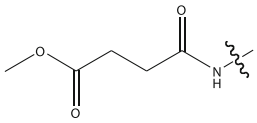	15	7.82
	B014	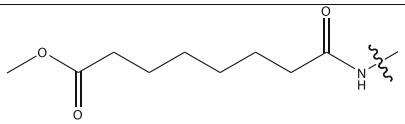	23	7.64
	B015	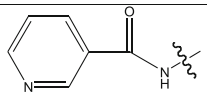	11	7.96
	***B016**	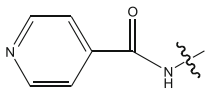	8	8.10
	B017	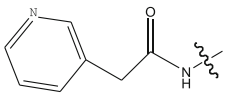	9	8.05

Table 1 (continued)

	B018	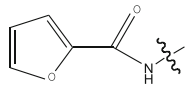	111	6.95
	B019	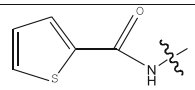	42	7.38
	B020	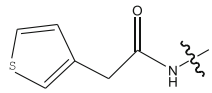	58	7.24
	***B021**	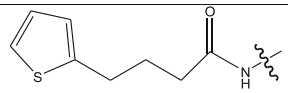	91	7.04
	B022	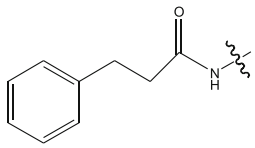	68	7.17
	B023	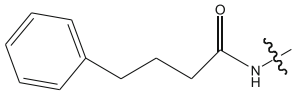	243	6.61
	B024	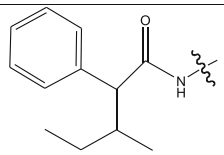	328	6.48
	B025	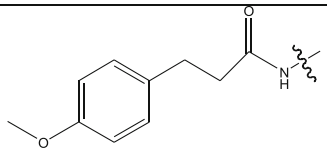	72	7.14
	***B026**	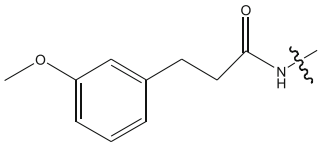	51	7.29
	B027	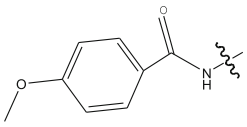	1365	5.86
	B028	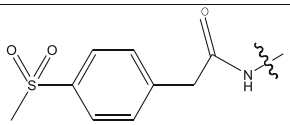	7	8.15
	B029	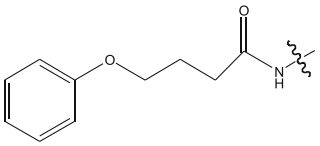	228	6.64
	B030	-CHO	14	7.85
	***B031**	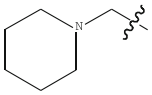	12	7.92

Table 1 (continued)

Structure C	No	R^2	R^4	X^5	IC_{50}(nM)	PIC_{50}
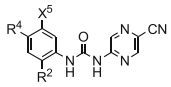	C032	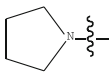	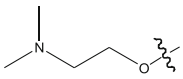	Cl	10	8.00
	C033	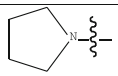	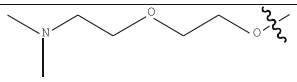	Cl	25	7.60
	C034	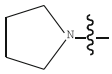	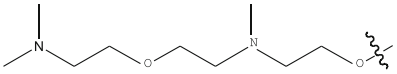	Cl	64	7.19
	C035	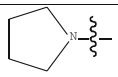	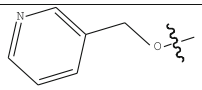	Cl	38	7.42
	***C036**	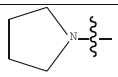	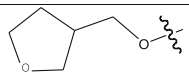	Cl	15	7.82
	C037	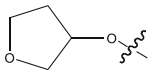	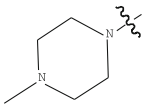	Cl	66	7.18
	C038	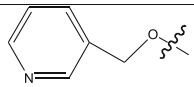	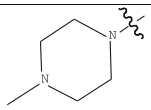	Cl	38	7.42
	C039	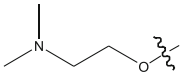	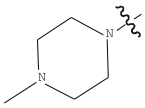	Cl	43	7.37
	C040	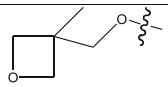	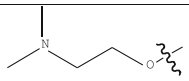	Cl	32	7.49
	***C041**	CH_3O	CHO	H	45	7.35
	C042	CH_3O	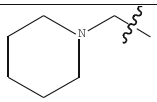	H	10	8.00
	C043	CH_3O	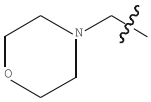	H	96	7.02
	C044	CH_3O	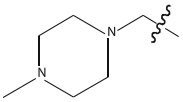	H	73	7.14
	C045	CH_3O	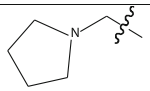	H	13	7.89
	***C046**	CH_3O	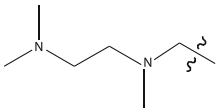	H	112	6.95
Structure D	**No**	**R**		**IC_{50}(nM)**	**PIC_{50}**	
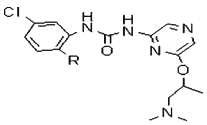	D047	H		26	7.59	
	D048	CH_3O		22	7.66	

Table 1 (continued)

Structure E	No	n=	X	IC_{50}(nM)	PIC_{50}
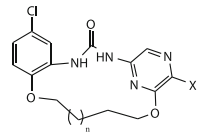	E049	2	H	10	8.00
	E050	2	CN	7	8.15
	***E051**	1	CN	6	8.22
	E052	3	CN	28	7.55

Structure F	No	R	IC_{50}(nM)	PIC_{50}
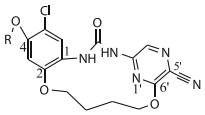	F053	H	6	8.22
	F054	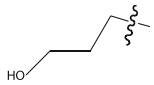	2	8.70
	F055	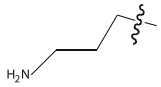	1	9.00
	***F056**	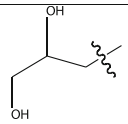	3	8.52
	F057	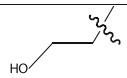	6	8.22
	F058	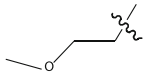	5	8.30
	F059	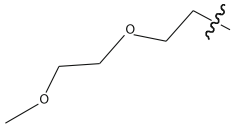	9	8.05
	F060	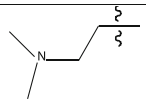	1	9.00
	***F061**	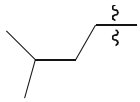	1060	5.97
	F062	Et	6	8.22
	F063		13	7.89
	F064	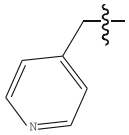	12	7.92
	F065	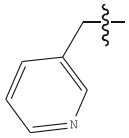	9	8.05
	***F066**	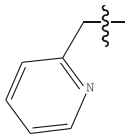	63	7.20

Table 1 (continued)

	F067	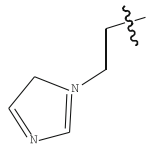	3	8.52
Structure G 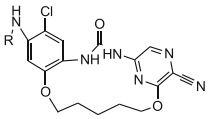	No	R	3	PIC_{50}
	G068	H	3	8.52
	G069	CH_3	2	8.70
	G070	CH_3CH_2	4	8.40
	***G071**	n-Bu	15	7.82
	G072	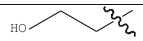	2	8.70
	G073		11	7.96
	G074	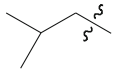	17	7.77
	G075	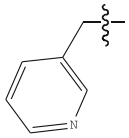	12	7.92
	***G076**	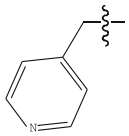	13	7.89
	G077	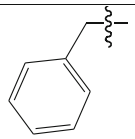	266	6.58
	G078	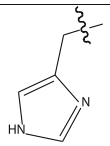	231	6.64
	G079	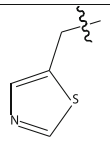	6	8.22
	G080	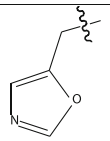	7	8.15
	***G081**	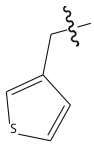	162	6.79

Table 1 (continued)

	G082	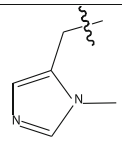	2	8.70
	G083		7	8.15
	G084	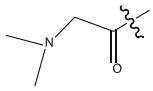	1	9.00
	G085	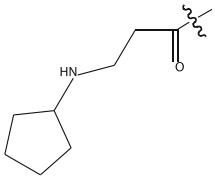	2	8.70
	***G086**	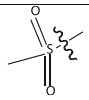	15	7.82
Structure H	No	R	**IC_{50}(nM)**	PIC_{50}
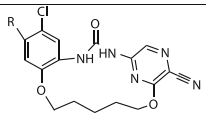	H087		7	8.15
	H088	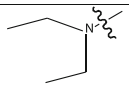	248	6.61
	H089	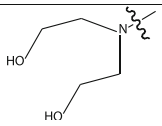	4	8.40
	H090	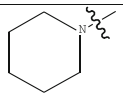	139	6.86
	***H091**	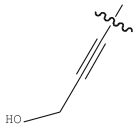	10	8.00
	H092	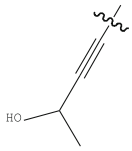	26	7.59
	H093	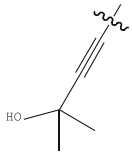	109	6.96

Table 1 (continued)

	H094	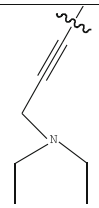	2	8.70
	H095	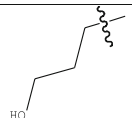	5	8.30
	***H096**	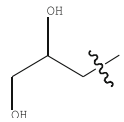	5	8.30
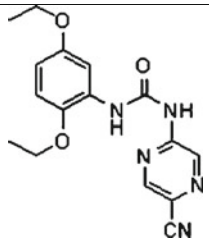	097	/	31	7.51
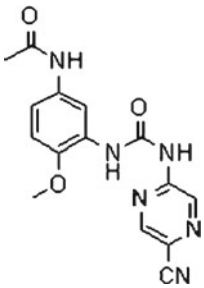	098	/	22	7.66
Structure I 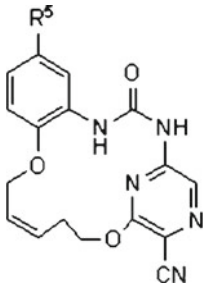	I099	-OH -OH	34	7.47
	I100	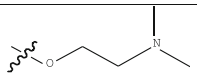	15	7.82
	***I101**		37	7.43
	I102	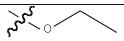	19	7.72
	I103	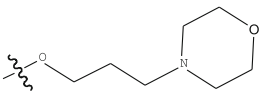	5	8.30
	I104	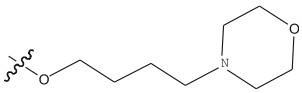	6	8.22
	I105	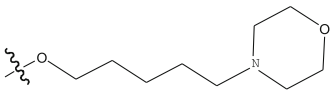	5	8.30
	***I106**	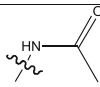	16	7.80
	I107	-Br	12	7.92

Table 1 (continued)

	I108	-H	12	7.92
	I109	-Cl	10	8.00
	I110	-Me	15	7.82
	***I111**	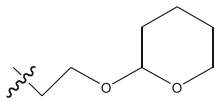	108	6.97
	I112	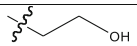	97	7.01
	I113	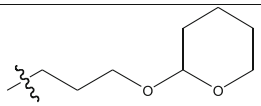	91	7.04
	I114	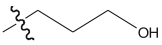	69	7.16
	I115	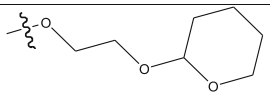	19	7.72
	***I116**	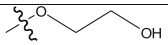	13	7.89
Structure J	J117		25	7.60
	J118	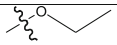	35	7.46
	J119	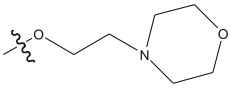	7	8.15
	J120	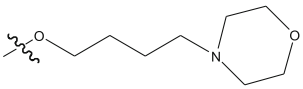	3	8.52
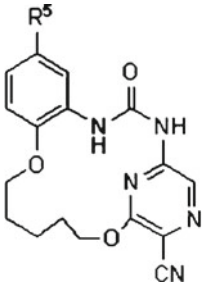	***J121**	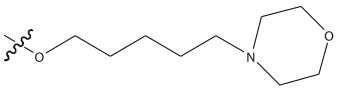	3	8.52
	J122	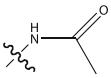	8	8.10
	J123	-Br	12	7.92
	J124	-H	16	7.80
	J125	-Cl	11	7.96
	***J126**	-Me	8	8.10
	J127	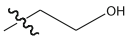	39	7.41
	J128	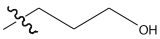	24	7.62
	J129	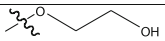	11	7.96
Structure K	K130	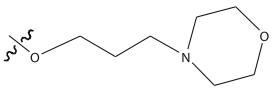	4	8.40
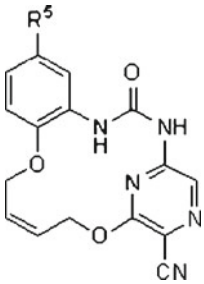	***K131**	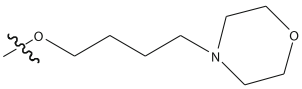	4	8.40
	K132	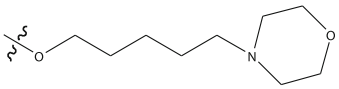	2	8.70
	K133	-Cl	5	8.30

Table 1 (continued)

Structure L 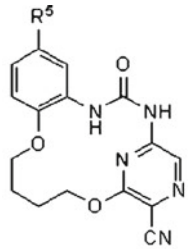	L134	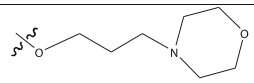	2	8.70
	L135	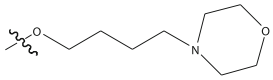	4	8.40
	***L136**	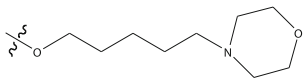	3	8.52
	L137	-Cl -Cl	6	8.22
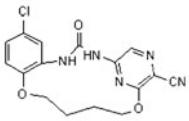	No	n=	**IC_{50}(nM)**	PIC_{50}
	M138	2	7	8.15
	M139	3	28	7.55
	N140	NH_2	0.3	9.52
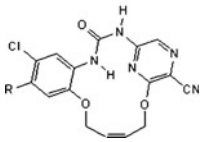	***N141**		2	8.70
	N142		2	8.70
	N143	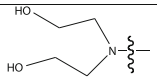	1	9.00
	N144	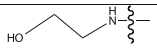	2	8.70
	N145	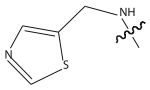	4	8.40
	***N146**	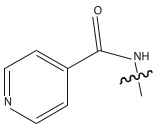	6	8.22
	N147	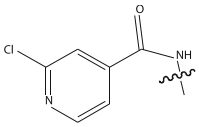	6	8.22
	N148	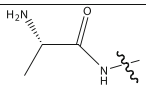	3	8.52
	N149	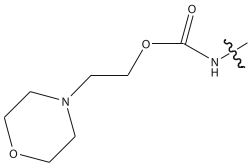	3	8.52
	N150	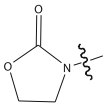	10	8.00
	***N151**	-OH -OH	0.3	9.52

Table 1 (continued)

	N152	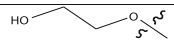	1	9.00
	N153	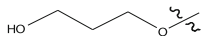	2	8.70
	N154	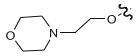	1	9.00
	N155	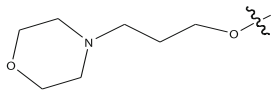	0.3	9.52
	***N156**	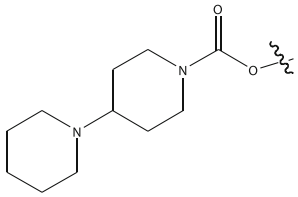	1	9.00
Structure O	O157	H	6	8.22
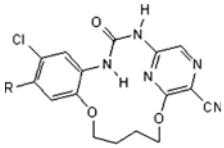	O158	NH_2	1	9.00
	O159		2	8.70
	O160		2	8.70

	***O161**	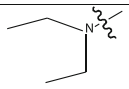	23	7.64
	O162	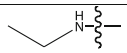	3	8.52
	O163	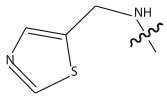	4	8.40
	O164	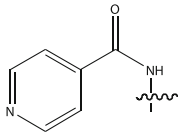	4	8.40
	O165	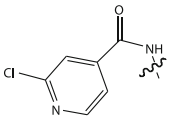	4	8.40
	***O166**	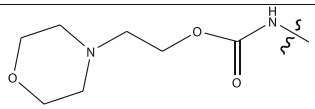	3	8.52
	O167	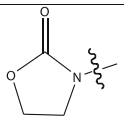	6	8.22
	O168	OH OH	0.3	9.52
	O169	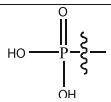	8	8.10
	O170		8	8.10

of Chk1 inhibitors. The grid spacing was set at 2Å and the region was calculated automatically by the program. In CoMFA descriptors, the steric (Lennard-Jones 6-12 potential) field and electrostatic (Coulombic potential) were probed using a default set of sp3 carbon probe atom having a charge of +1 and a van der Waals radius (VDR) of 1.52 Å with distance-dependent dielectric at each lattice point [6]. The column filtering (minimums) was set to 2 kcal mol^{-1}. Both energy calculations were truncated to 30 kcal mol^{-1} for all grid points. In CoMSIA model, the same grids constructed for the CoMFA fields calculation were used for CoMSIA fields calculation, and five physicochemical properties—steric, electrostatic, hydrophobic, hydrogen-bond donor and acceptor fields—were calculated with the set of sp3-carbon probe atom under charge +1, VDR radius 1.52 and attenuation factor as 0.3, respectively. The minimum-sigma was set to 2.0 kcal mol^{-1}, and the CoMFA/CoMSIA results were graphically interpreted by field contribution maps using the "STDEV*COEFF" field type.

Molecular docking

The 174 ligands were docked into the catalytic active site of the Chk1 by the AutoDock (V4.0) [22] program. Apparently binding mode was explored between these 174 ligands and the receptor. All the chemicals and the receptor were prepared by the AutoDock Tools1.4.5 (ADT) program. After deleting all the water molecules and its ligands from the original protein, polar hydrogen atoms were added and Kollman charges [23], atomic solvation parameters and fragmental volumes were assigned to the protein using AutoDock Tools (ADT). Gasteiger partial charges [24] were added to the inhibitors, and non-polar hydrogen atoms were merged in docking calculations. All torsions were allowed to rotate during docking. The parameters of the grid box for each ligand—receptor were disposed of in PDBBOX scripting program.

The grid maps were generated by the auxiliary program AutoGrid. The grid dimensions were $45\times45\times45Å^3$ with points separated by 0.375Å. Each grid was centered at the crystal structure of the corresponding inhibitors. The distance-dependent dielectric permittivity of Mehler and Solmajer [25] was applied to calculate the electrostatic grid maps. Lennard–Jones parameters 12-10 and 12-6 with the program, were used for modeling van der Waals interactions and H-bonds, respectively. For all ligands, random starting positions, random orientations and torsions were used, and the translation, quaternion and torsion steps were taken from default values in AutoDock. The Lamarckian genetic algorithm, the pseudo-Solis and Wets methods were applied for minimization using default parameters. The number of docking runs and the population in the genetic algorithm were 50, the energy evaluations were 250 000 and the maximum number of iterations 27 000. After docking, the 50 solutions were clustered into groups with RMS deviations lower than 1.0 Å. The clusters were ranked by the lowest energy representative of each cluster. The complexes of ligands with CHK1 resulting from molecular docking were further structurally optimized modifying the atom type and adding Gasteiger–Hückel partial charges.

PLS regression analysis

Partial least squares (PLS) has been universal application of 3D-QSAR methods [7] for analyzing the significant statistical relationship of inhibitor testing set in CoMFA and CoMSIA models. In this research, the CoMFA and CoMSIA descriptors were considered as independent variables. All the experimental bioactive pIC_{50} values were considered as the target variables in PLS regression analyses to derive 3D-QSAR models under the standard implementation in the SYBYL package. Leave one out (LOO) [26] option was used as cross-validation in PLS to obtain the optimal number of components used subsequently in the final analysis. The cross-validated coefficient q^2 was calculated by this using equation, where Ypred, Yactu, and Ymean were predicted, actual, and mean values of the target property (pIc50), respectively.

$$q^2 = 1 - \frac{\sum (Y_{pred} - Y_{actu})^2}{\sum (Y_{actu} - Y_{mean})^2} \quad (1)$$

In addition, the statistical significance of the models was described by the F and probability value computed according to the definitions in SYBYL. The final model was constructed with the optimum number of components equal to that yielding the highest q^2.

Results and discussion

3D-QSAR models

Using a series of Chk1 inhibitors, possessing receptor antagonistic activity, CoMFA and CoMSIA 3D-QSAR models were derived. The statistical parameters obtained from CoMFA and CoMSIA analysis were listed in Table 2. As shown in Table 2, the best predictions were gained by the CoMFA and CoMSIA, which indicated the established 3D-QSAR models were reliable and able to accurately predict binding affinities of new derivatives. In CoMFA, in training set the PLS analysis of Chk1 inhibitors with 4 principal components showed cross-validated q^2 of 0.572 and non cross-validated r^2 value of 0.873; the standard error and F value were 0.238 and 152.304, respectively; the steric and electrostatic contributions were shown to be 55.8% and

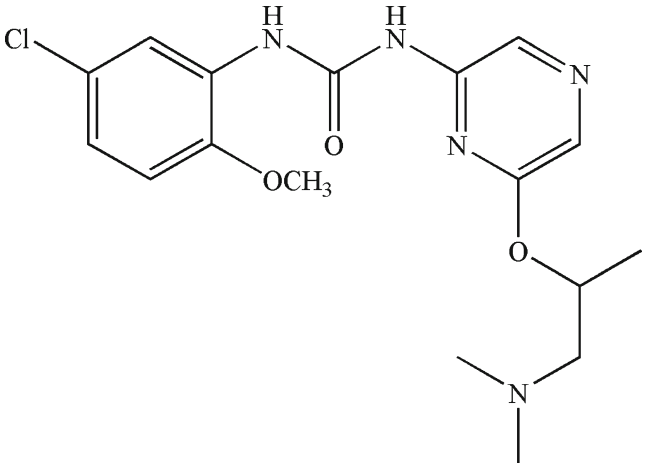

Fig. 1 A structure of A/Q77A1001 as a template

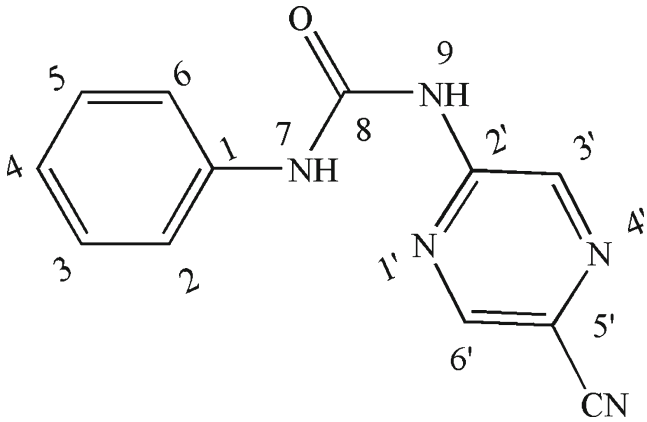

Fig. 3 Common structure built on A/Q77A1001, the figures indicate the atoms selected as the common substructure

44.2%. Consequently, the steric field and the electrostatic field had almost the same contribution to the model, demonstrating that the steric and electrostatic interactions of the molecules with the receptor could be two crucial factors for the antagonistic activity of Chk1. The date of CoMFA analysis indicated a reasonable statistical correlation and internal predictability of CoMFA model. Besides the correlation between the actual and the predicted values from the final CoMFA model is listed in Fig. 5A.

In CoMSIA, detailed hydrophobic, hydrogen-bond donor and acceptor descriptors in addition to steric and electrostatic fields were defined and employed. Using all compounds in training set and all the five descriptors, a model with high q^2 value of 0.599 for 4 components and a conventional r^2 value of 0.897, was built. The SEE and F value were 0.216 and 189.517, respectively. Besides the steric (S), electrostatic (E), hydrophobic (H), hydrogen-bond donor (D) and hydrogen-bond acceptor (A) field descriptor contributed 12.6%, 33.7%, 24.9%, 13.7% and 15.1% respectively. The results of CoMSIA analysis were also summarized in Table 2, which indicated that the CoMSIA model was successfully constructed and reliable. Predicted activities via this model versus experimental activities of inhibitors were expressed in Fig. 5B. Obviously, a conclusion can be drawn from Fig. 5 that the predicted pIC50 values gained from CoMFA and CoMSIA models are consistent with the actual data. All the predicted activities of the 174 compounds for both CoMFA and CoMSIA models were also shown in Table 3. Of which, 34 compounds as an external test set were selected to further validate the 3D-QSAR models. The predictions of the training and test set compounds were both

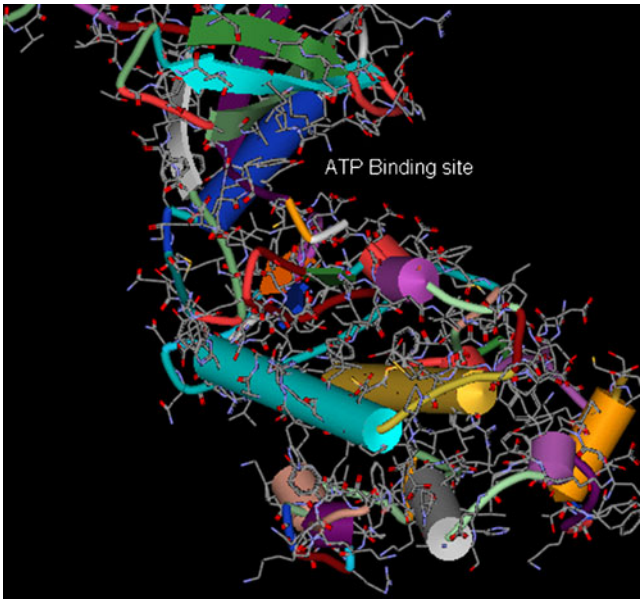

Fig. 2 Structure of Chk1, with its activate site

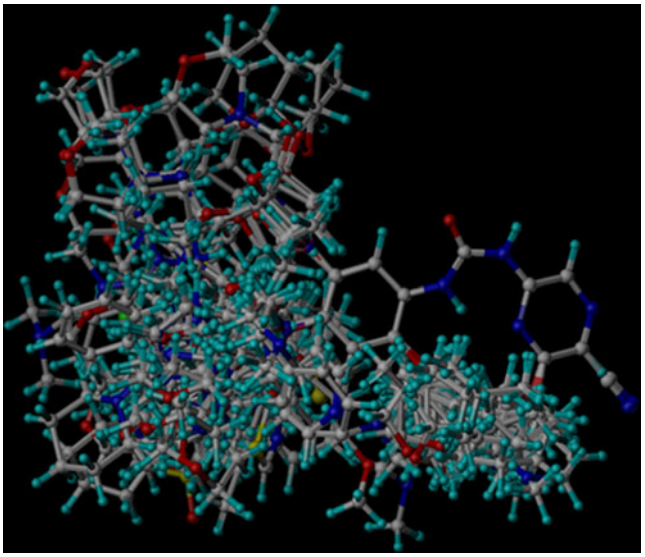

Fig. 4 The alignment of the test set and training set, including all the chemicals available in the research

Table 2 Statistical parameters of CoMFA and CoMSIA models of the training sets

	NOC	q^2	r^2	SEE	F	Fraction of field contribution				
						S	E	H	D	A
CoMFA	4	0.572	0.873	0.238	152.304	0.558	0.442			
CoMSIA	4	0.599	0.897	0.216	189.517	0.126	0.337	0.249	0.137	0.151

q^2: Leave one out (LOO) cross-validated correlation coefficient; ONC: optimum number of components; r^2: non cross-validated correlation coefficient; SEE: standard error of estimate. F: F-test value; S, E, H, A, D: steric, electrostatic, hydrophobic, as well as hydrogen-bond acceptor and donor fields, respectively.

successfully performed by CoMFA and CoMSIA models. The deviations of the predicted pIC50 values from the corresponding experimental pIC50 values are less than 1 log unit in two models.

Mapping of CoMFA and sCoMSIA models

The visualization of the results as 3D coefficient contour plots is one of the attractive advantages of the CoMFA and CoMSIA modeling. The contour maps were formed as scalar products of coefficients and standard deviation, related to each CoMFA or CoMSIA column. And the maps generated depict regions having scaled coefficients greater than 80% (favored) or less than 20% (disfavored), which showed regions where variations of steric, electrostatic, hydrophilic, hydrogen-bond donor or acceptor nature in the structural features of the different molecules included in the training set lead to increases or decreases in the activity. Based on the alignment of the conformations of several compounds (such as 9, 28, 35, 82, 93, 121, 151, 155 and 168), the five fields of CoMFA and CoMSIA models for the analysis were emerged as contour plots in Fig. 6.

All lattice points, where the QSAR linked changes in the compounds' field values with changes in biological potency, were surrounded by the colored polyhedral in these maps. Green-colored regions shown by the CoMFA contour plots expressed that increasing steric can enhance activity, while the inhibitor activity can be decreased in yellow colored regions where steric bulk is augmented (Fig. 6A). As Fig. 6A shows, two green polyhedrons, around the substituent linking with the 2-, 6'-position and below the substituents linking with 4-position, may reveal that the more bulky substituents in these areas are, the more biological activities increase. In the area between the 4- position and 5-position several big regions of yellow contour implied that more bulky substituent will significantly decrease the biological activities.

Regions where increased negative charge is favorable for antagonist activity are colored red, while the regions where increased positive-charge is favorable for antagonist activities are shown in blue (Fig. 6B). In the Fig. 6B, the areas above the 2-, 6'-position, and the regions above and below the substituent between 4-position and 5-position, which dyed red, indicate that negatively charged substituent may enhance the antagonist activity. While a big blue contour, where less negatively charged substituent will greatly

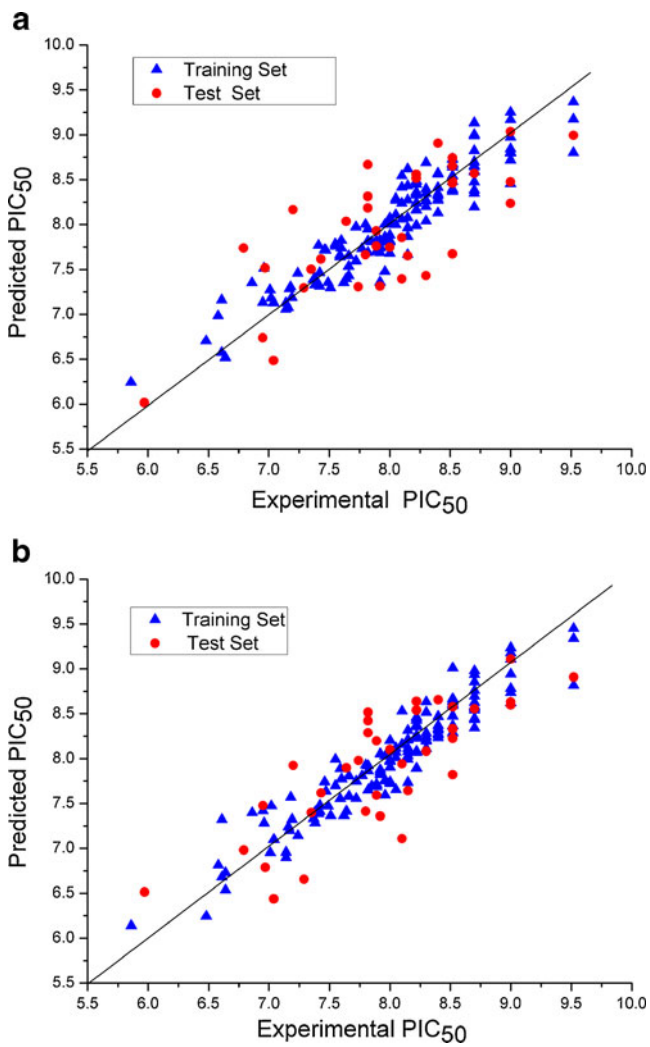

Fig. 5 Correlation between the actual and predicted activities of 3D-QSAR models (A: CoMFA model; B: CoMSIA model) for the training set and test set. "▲" on behalf of the training set, "●" on behalf of test set

Table 3 Comparison of actual and predicted pIC50 values of all 174 compounds for CoMFA and CoMSIA models

No.	pIC_{50}	CoMFA		CoMSIA		No.	pIC_{50}	CoMFA		CoMSIA	
		predicted	residuals	predicted	residuals			predicted	residuals	predicted	residuals
001*	**8.52**	**7.673**	**0.847**	**7.821**	**0.699**	088	6.61	7.161	−0.551	7.322	−0.712
002	8.30	8.039	0.261	8.114	0.186	089	8.40	8.13	0.27	8.232	0.168
003	8.00	8.006	−0.006	8.202	−0.202	090	6.86	7.352	−0.492	7.397	−0.537
004	8.10	8.238	−0.138	8.16	−0.06	**091***	**8.00**	**7.747**	**0.253**	**8.1**	**−0.1**
005	8.15	7.867	0.283	7.994	0.156	092	7.59	7.638	−0.048	7.888	−0.298
006*	**8.15**	**7.652**	**0.498**	**7.644**	**0.506**	093	6.96	7.514	−0.554	7.282	−0.322
007	7.38	7.402	−0.022	7.407	−0.027	094	8.70	8.475	0.225	8.437	0.263
008	8.30	8.2	0.1	8.517	−0.217	095	8.30	8.272	0.028	8.193	0.107
009	8.52	8.392	0.128	8.475	0.045	**096***	**8.30**	**7.431**	**0.869**	**8.082**	**0.218**
010	7.66	7.653	0.007	7.806	−0.146	097	7.51	7.295	0.215	7.365	0.145
011*	**7.74**	**7.307**	**0.433**	**7.98**	**−0.24**	098	7.66	7.432	0.228	7.584	0.076
012	8.05	8.11	−0.06	8.011	0.039	099	7.47	7.715	−0.245	7.637	−0.167
013	7.82	7.952	−0.132	7.864	−0.044	100	7.82	7.689	0.131	7.652	0.168
014	7.64	7.397	0.243	7.414	0.226	**101***	**7.43**	**7.615**	**−0.185**	**7.618**	**−0.188**
015	7.96	7.478	0.482	7.594	0.366	102	7.72	7.595	0.125	7.556	0.164
016*	**8.10**	**7.395**	**0.705**	**7.109**	**0.991**	103	8.30	8.396	−0.096	8.243	0.057
017	8.05	8.292	−0.242	8.072	−0.022	104	8.22	8.337	−0.117	8.08	0.14
018	6.95	7.134	−0.184	7.417	−0.467	105	8.30	8.347	−0.047	8.285	0.015
019	7.38	7.327	0.053	7.285	0.095	**106***	**7.80**	**7.663**	**0.137**	**7.413**	**0.387**
020	7.24	7.459	−0.219	7.143	0.097	107	7.92	7.754	0.166	7.875	0.045
021*	**7.04**	**6.484**	**0.556**	**6.438**	**0.602**	108	7.92	7.685	0.235	7.82	0.1
022	7.17	7.285	−0.115	7.2	−0.03	109	8.00	7.808	0.192	7.982	0.018
023	6.61	6.575	0.035	6.68	−0.07	110	7.82	7.818	0.002	7.922	−0.102
024	6.48	6.706	−0.226	6.244	0.236	**111***	**6.97**	**7.518**	**−0.548**	**6.789**	**0.181**
025	7.14	7.057	0.083	6.957	0.183	112	7.01	7.273	−0.263	6.953	0.057
026*	**7.29**	**7.295**	**−0.005**	**6.655**	**0.635**	113	7.04	7.129	−0.089	7.098	−0.058
027	5.86	6.244	−0.384	6.139	−0.279	114	7.16	7.076	0.084	7.239	−0.079
028	8.15	8.432	−0.282	8.08	0.07	115	7.72	7.974	−0.254	7.749	−0.029
029	6.64	6.522	0.118	6.536	0.104	**116***	**7.89**	**7.761**	**0.129**	**7.593**	**0.297**
030	7.85	7.811	0.039	7.695	0.155	117	7.60	7.825	−0.225	7.774	−0.174
031*	**7.92**	**7.313**	**0.607**	**7.36**	**0.56**	118	7.46	7.717	−0.257	7.741	−0.281
032	8.00	7.679	0.321	7.725	0.275	119	8.15	8.076	0.074	8.213	−0.063
033	7.60	7.739	−0.139	7.771	−0.171	120	8.52	8.371	0.149	8.366	0.154
034	7.19	7.188	0.002	7.323	−0.133	**121***	**8.52**	**8.741**	**−0.221**	**8.226**	**0.294**
035	7.42	7.464	−0.044	7.481	−0.061	122	8.10	8.06	0.04	8.158	−0.058
036*	**7.82**	**8.67**	**−0.85**	**8.423**	**−0.603**	123	7.92	7.74	0.18	7.849	0.071
037	7.18	7.306	−0.126	7.571	−0.391	124	7.80	8.001	−0.201	7.929	−0.129
038	7.42	7.313	0.107	7.41	0.01	125	7.96	8.001	−0.041	8.029	−0.069
039	7.37	7.389	−0.019	7.332	0.038	**126***	**8.10**	**7.856**	**0.244**	**7.942**	**0.158**
040	7.49	7.354	0.136	7.471	0.019	127	7.41	7.769	−0.359	7.386	0.024
041*	**7.35**	**7.503**	**−0.153**	**7.397**	**−0.047**	128	7.62	7.352	0.268	7.364	0.256
042	8.00	7.884	0.116	7.741	0.259	129	7.96	7.864	0.096	7.76	0.2
043	7.02	7.183	−0.163	7.473	−0.453	130	8.40	8.285	0.115	8.471	−0.071
044	7.14	7.127	0.013	6.899	0.241	**131***	**8.40**	**8.907**	**−0.507**	**8.656**	**−0.256**
045	7.89	7.701	0.189	7.689	0.201	132	8.70	8.351	0.349	8.56	0.14
046*	**6.95**	**6.739**	**0.211**	**7.477**	**−0.527**	133	8.30	8.691	−0.391	8.633	−0.333
047	7.59	7.66	−0.07	7.554	0.036	134	8.70	8.659	0.041	8.541	0.159

Table 3 (continued)

No.	pIC_{50}	CoMFA		CoMSIA		No.	pIC_{50}	CoMFA		CoMSIA	
		predicted	residuals	predicted	residuals			predicted	residuals	predicted	residuals
048	7.66	7.534	0.126	7.579	0.081	135	8.40	8.563	−0.163	8.338	0.062
049	8.00	8.074	−0.074	7.97	0.03	**136***	**8.52**	**8.654**	**−0.134**	**8.334**	**0.186**
050	8.15	8.274	−0.124	8.316	−0.166	137	8.22	8.359	−0.139	8.374	−0.154
051*	**8.22**	**8.516**	**−0.296**	**8.539**	**−0.319**	138	8.15	8.077	0.073	8.116	0.034
052	7.55	7.76	−0.21	7.7	−0.15	139	7.55	7.785	−0.235	7.994	−0.444
053	8.22	8.45	−0.23	8.458	−0.238	140	9.52	9.174	0.346	9.337	0.183
054	8.70	8.589	0.111	8.697	0.003	**141***	**8.70**	**8.571**	**0.129**	**8.555**	**0.145**
055	9.00	8.805	0.195	9.108	−0.108	142	8.70	9.004	−0.304	8.855	−0.155
056*	**8.52**	**8.483**	**0.037**	**8.33**	**0.19**	143	9.00	8.455	0.545	8.782	0.218
057	8.22	8.162	0.058	8.355	−0.135	144	8.70	8.991	−0.291	8.936	−0.236
058	8.30	8.261	0.039	8.21	0.09	145	8.40	8.323	0.077	8.47	−0.07
059	8.05	7.999	0.051	7.655	0.395	**146***	**8.22**	**8.559**	**−0.339**	**8.638**	**−0.418**
060	9.00	8.844	0.156	8.737	0.263	147	8.22	8.481	−0.261	8.428	−0.208
061*	**5.97**	**6.016**	**−0.046**	**6.513**	**−0.543**	148	8.52	8.642	−0.122	8.591	−0.071
062	8.22	8.33	−0.11	7.892	0.328	149	8.52	8.542	−0.022	8.611	−0.091
063	7.89	7.825	0.065	7.715	0.175	150	8.00	7.823	0.177	7.904	0.096
064	7.92	7.823	0.097	8.053	−0.133	**151***	**9.52**	**8.995**	**0.525**	**8.908**	**0.612**
065	8.05	8.271	−0.221	8.119	−0.069	152	9.00	8.72	0.28	8.62	0.38
066*	**7.20**	**8.167**	**−0.967**	**7.924**	**−0.724**	153	8.70	8.601	0.099	8.586	0.114
067	8.52	8.67	−0.15	8.667	−0.147	154	9.00	9.251	−0.251	9.178	−0.178
068	8.52	8.73	−0.21	9.009	−0.489	155	9.52	9.368	0.152	9.451	0.069
069	8.70	8.7	0	8.575	0.125	**156***	**9.00**	**8.476**	**0.524**	**8.631**	**0.369**
070	8.40	8.272	0.128	8.28	0.12	157	8.22	7.989	0.231	8.256	−0.036
071*	**7.82**	**8.314**	**−0.494**	**8.288**	**−0.468**	158	9.00	8.975	0.025	9.235	−0.235
072	8.70	8.195	0.505	8.343	0.357	159	8.70	8.382	0.318	8.451	0.249
073*	7.96	7.805	0.155	7.754	0.206	160	8.70	8.824	−0.124	8.759	−0.059
074	7.77	7.732	0.038	7.81	−0.04	**161***	**7.64**	**8.036**	**−0.396**	**7.898**	**−0.258**
075	7.92	7.358	0.562	7.821	0.099	162	8.52	8.478	0.042	8.288	0.232
076*	**7.89**	**7.929**	**−0.039**	**8.197**	**−0.307**	163	8.40	8.573	−0.173	8.37	0.03
077	6.58	6.984	−0.404	6.814	−0.234	164	8.40	8.342	0.058	8.262	0.138
078	6.64	6.515	0.125	6.73	−0.09	165	8.40	8.413	−0.013	8.317	0.083
079	8.22	8.24	−0.02	8.227	−0.007	**166***	**8.52**	**8.461**	**0.059**	**8.577**	**−0.057**
080	8.15	7.965	0.185	8.032	0.118	167	8.22	7.986	0.234	8.071	0.149
081*	**6.79**	**7.738**	**−0.948**	**6.981**	**−0.191**	168	9.52	8.801	0.719	8.817	0.703
082	8.70	8.645	0.055	8.626	0.074	169	8.10	8.416	−0.316	8.156	−0.056
083	8.15	8.621	−0.471	8.205	−0.055	170	8.10	8.545	−0.445	8.529	−0.429
084	9.00	8.796	0.204	8.941	0.059	**171***	**9.00**	**9.037**	**−0.037**	**9.11**	**−0.11**
085	8.70	9.134	−0.434	8.979	−0.279	172	8.52	8.681	−0.161	8.638	−0.118
086*	**7.82**	**8.185**	**−0.365**	**8.516**	**−0.696**	173	9.00	9.168	−0.168	9.107	−0.107
087	8.15	7.665	0.485	7.735	0.415	**174***	**9.00**	**8.237**	**0.763**	**8.596**	**0.404**

* Compounds of the testing set

improve the biological activities in the area, is shown in the 4-position.

The results of steric and electrostatic regions of CoMSIA were shown in Fig. 6C and Fig. 6D. Compared with the result of CoMFA, there is little difference between them. As shown in Fig. 6C and Fig. 6D, small substituents are favorable for antagonist activity in the area between 4- position and 5- position; while introducing bulky substituent into the regions around the substituent linking with the 2-, 6'-position and below the substituent linking with 4-position will

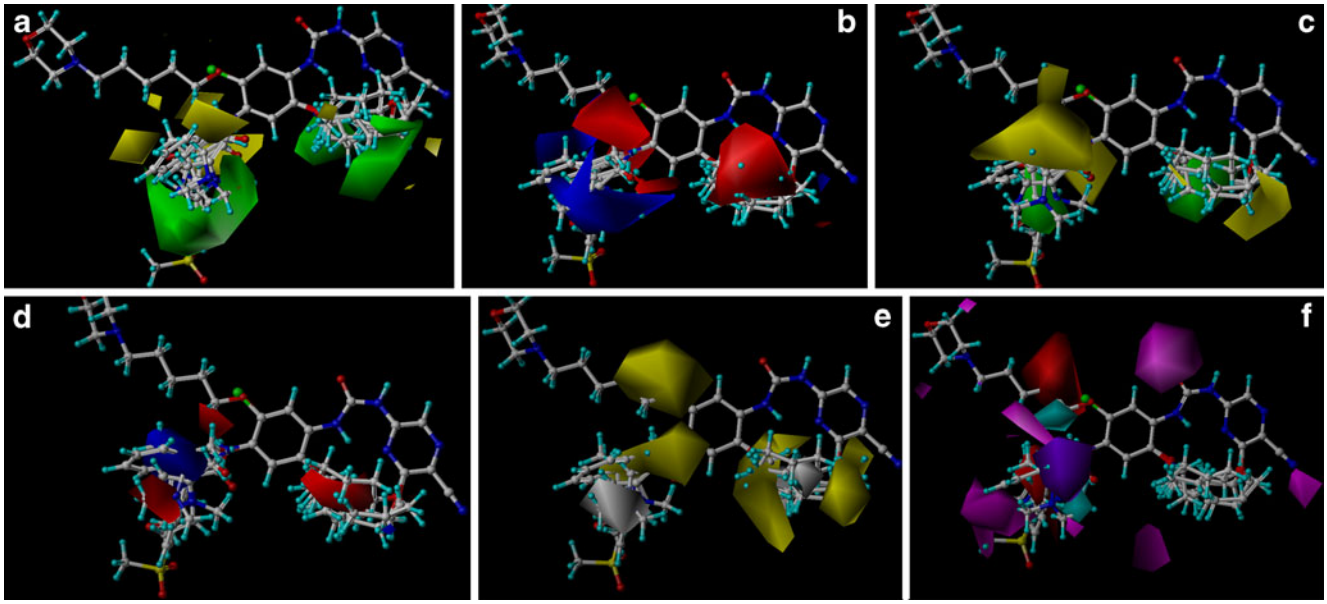

Fig. 6 CoMFA (**A** and **B**) and CoMSIA (**C**, **D**, **E**, and **F**) contour maps. Steric fields: green contours indicate regions where bulky groups increase activity, while yellow contours indicate regions where bulky groups decrease activity; electrostatic fields: blue contours represent regions where positive-charge groups increase activity, while red contours represent regions where negative-charge groups increase activity; Hydrophobic fields: the yellow and gray contours indicate favorable and unfavorable hydrophobic groups; Hydrogen bond donor contour map: the cyan and purple contours indicate favorable and unfavorable hydrogen bond donor groups; Hydrogen bond acceptor contour map: the magenta and red contours indicate favorable and unfavorable hydrogen bond acceptor groups. Compound 52 was superposed as the reference molecules in the maps. The maps generated depict regions having scaled coefficients greater than 80% (favored) or less than 20% (disfavored)

increase the antagonist activity. In addition, electropositive substituents are favorable for antagonist activity in the 4-position, yet strong electronegative substituent may enhance the antagonist activity in the areas above the 2-, 6'-position, and the regions above and below the substituent between 4-position and 5-position.

The CoMSIA contour plots express yellow-colored regions, where increased hydrophobic interaction is related to enhance biological activities. While in white-colored regions decreased hydrophilic interaction is associated with increased biological activities. As shown in Fig. 3E, there are large regions of yellow contour around 2, 4, 5 and 6'-position, respectively, which indicates that adding hydrophobic substituents can increase the antagonist activity. However, two big white-colored polyhedrons around the ring between 2- position and 6'-position and near 4-position illustrate that adding hydrophobic groups at these positions would be detrimental to antagonist activity, and hydrophilic groups are in favor of improving antagonist activity.

The cyan and purple regions mean that hydrogen-bond donor substituents are favorable and unfavorable for antagonist activity, respectively. And the regions where hydrogen-bond acceptor substituents are favorable or unfavorable for antagonist activity are indicated in magenta or red, as Fig. 3F shows. The large area of purple contours around 4-position suggests hydrogen-bond donor substituents in these positions will be unfavorable for antagonist activity. While two red contours around the 5-position and far away from 4-position indicate that hydrogen-bond acceptor substituents will decrease the biological activities in the region. Besides, several magenta contours in the -CN group of 5-position and above the carbonyl group indicate that hydrogen-bond acceptor substituents are unfavorable for the antagonist activity. However,t a big red region around 4 and 5-position signified that hydrogen-bond acceptor substituents are favorable for the antagonist activity.

To sum up, the research about CoMFA and CoMSIA based on the ligands indicates that inhibitors with large bulk, strongly hydrophobic and powerfully electronegative substituents may increase the activity on the 3 and 6'-position, and bringing in properly small bulk, weakly electronegative, and powerfully hydrophilic substituents on the 4-position may also be favorable to the antagonist activity. Besides it is favorable for the antagonist activity to place hydrogen-bond acceptor substituents (such as N,O) on 4-position.

Interactions between inhibitors and Chk1 binding pocket

A/Q77A1001 was removed from the active site and docked back into the binding pocket before docking using AUTODOCK4.0. The results were shown in Fig. 7A. The protocol

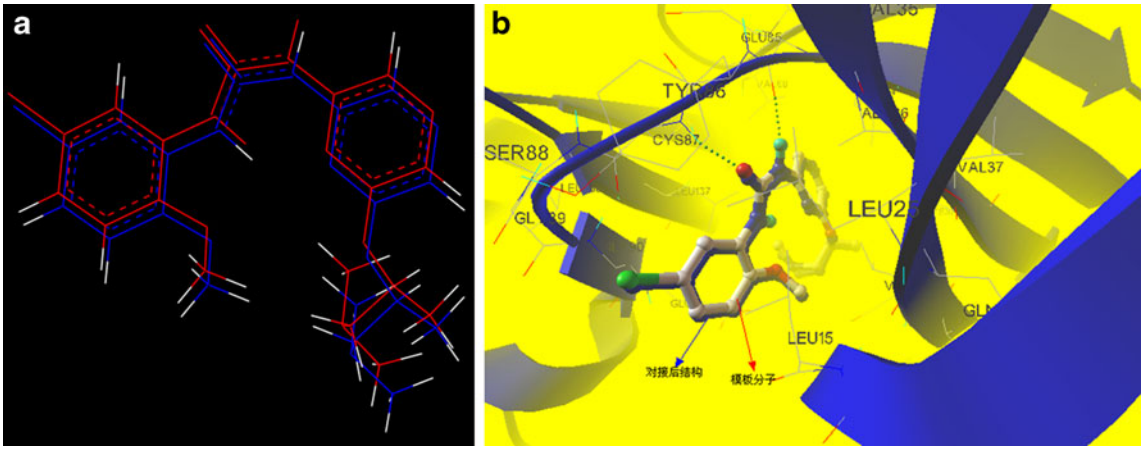

Fig. 7 (**A**) Conformational comparison of A/Q77A1001 (blue) from the crystal structure (by atom type color) and that from the autodock4.0 result (red). (**B**) Conformations the CHk1 binding site

and preferences of docking were validated before docking all inhibitors into the active sites of CHK1. In order to determine the credible binding conformations of these inhibitors, all inhibitors were docked into the active site. The root mean square deviation (RMSD) between the predicted conformation and the observed X-ray crystallographic conformation of A/Q77A1001 was 0.65Å (Fig. 7B). This RMSD value was small, which suggested that the parameter set was rational for the AutoDock simulation to redo the X-ray structure. Consequently, the parameter set and the AutoDock method could be competent to other inhibitors to search their binding conformations.

The docked conformation for each molecule was chosen on the basis of the grid score which was based on an estimation of van der Waal attractive, van der Waal dispersive and Columbic electrostatic energies. Using the flexible docking strategy, all the compounds were docked into the ATP binding site and were superimposed in the active pocket. The docked conformations of all compounds using this method were shown in Fig. 8A and Fig. 8B. The docked conformations were used to develop receptor-based model, serving as a very good starting point for carrying out 3D-QSAR modeling, in that the alignment of compound structures plays a crucial role in developing successful 3D-QSAR models. As shown in Fig. 8A and Fig. 8B, molecules after docking adopted reasonable conformations and no collision with the active pocket occurred.

Molecular docking based 3D-QSAR models

The predicted activities of all 174 compounds for both of CoMFA and CoMSIA models were listed in Table 4. The results of CoMFA and CoMSIA analysis of the training set were summarized in Table 5. The CoMFA model was obtained with LOO cross-validation q^2 and non-cross validated r^2 values of 0.501 and 0.887, respectively. The electrostatic and steric contributions are 55.4% and 44.6%, respectively, which indicated that the electrostatic field had more influence than the steric field to the model, demonstrating the electrostatic interactions of the molecules with the receptor could be a main factor for CHK1 antagonistic activity. CoMSIA

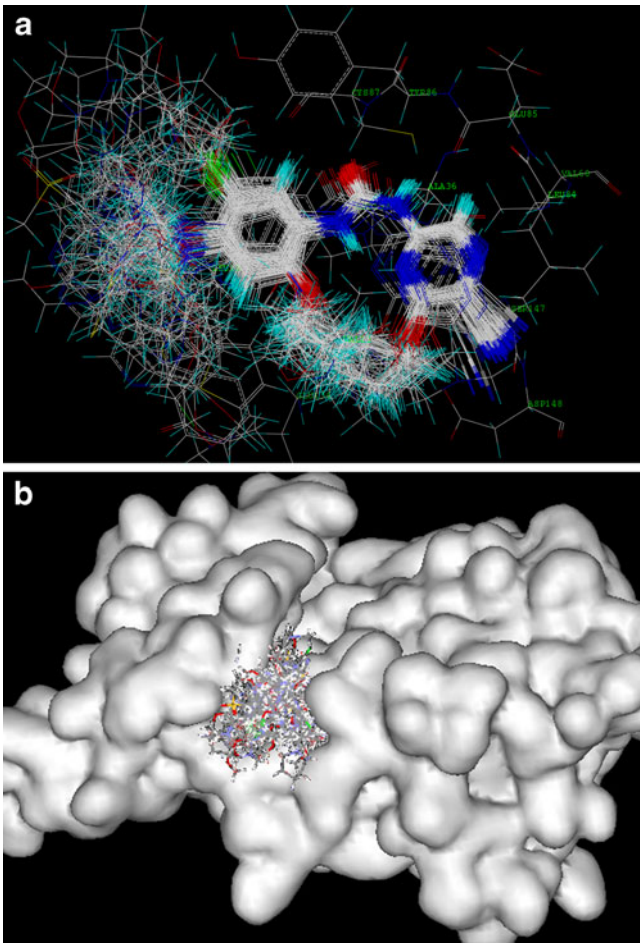

Fig. 8 (**A**) all the inhibitors based on docking. (**B**) All the docking inhibitors in the receptor-binding pocket

Table 4 Comparison of actual and predicted pIC50 values of all 140 compounds for CoMFA and CoMSIA models

No.	pIC_{50}	CoMFA		CoMSIA		No.	pIC_{50}	CoMFA		CoMSIA	
		predict	deviation	predict	deviation			predict	deviation	predict	deviation
001*	**8.52**	**8.091**	**0.429**	**8.522**	**−0.002**	088	6.61	7.195	−0.585	7.373	−0.763
002	8.30	7.84	0.46	8.083	0.217	089	8.40	8.186	0.214	8.615	−0.215
003	8.00	7.86	0.14	8	0	090	6.86	7.004	−0.144	7.102	−0.242
004	8.10	8.033	0.067	8.116	−0.016	**091***	**8.00**	**8.226**	**−0.226**	**8.214**	**−0.214**
005	8.15	7.919	0.231	8.127	0.023	092	7.59	7.648	−0.058	7.492	0.098
006*	**8.15**	**7.979**	**0.171**	**7.558**	**0.592**	093	6.96	7.132	−0.172	7.257	−0.297
007	7.38	7.525	−0.145	7.591	−0.211	094	8.70	8.65	0.05	8.314	0.386
008	8.30	8.408	−0.108	8.209	0.091	095	8.30	8.322	−0.022	8.213	0.087
009	8.52	8.261	0.259	8.075	0.445	**096***	**8.30**	**8.299**	**0.001**	**8.495**	**−0.195**
010	7.66	7.742	−0.082	7.939	−0.279	097	7.51	7.566	−0.056	7.727	−0.217
011*	**7.74**	**7.047**	**0.693**	**7.588**	**0.152**	098	7.66	7.764	−0.104	7.882	−0.222
012	8.05	8.234	−0.184	8.249	−0.199	099	7.47	7.619	−0.149	7.87	−0.4
013	7.82	7.762	0.058	8.077	−0.257	100	7.82	7.704	0.116	7.743	0.077
014	7.64	7.748	−0.108	7.578	0.062	**101***	**7.43**	**7.644**	**−0.214**	**7.985**	**−0.555**
015	7.96	7.518	0.442	7.895	0.065	102	7.72	7.552	0.168	7.868	−0.148
016*	**8.10**	**7.582**	**0.518**	**7.379**	**0.721**	103	8.30	8.294	0.006	8.211	0.089
017	8.05	8.068	−0.018	8.051	−0.001	104	8.22	7.968	0.252	7.947	0.273
018	6.95	7.197	−0.247	7.066	−0.116	105	8.30	8.391	−0.091	8.241	0.059
019	7.38	7.419	−0.039	6.925	0.455	**106***	**7.80**	**7.779**	**0.021**	**7.553**	**0.247**
020	7.24	6.929	0.311	7.003	0.237	107	7.92	7.853	0.067	8.079	−0.159
021*	**7.04**	**7.756**	**−0.716**	**7.306**	**−0.266**	108	7.92	7.794	0.126	7.917	0.003
022	7.17	7.28	−0.11	7.15	0.02	109	8.00	8.008	−0.008	8.089	−0.089
023	6.61	6.782	−0.172	6.525	0.085	110	7.82	7.681	0.139	7.843	−0.023
024	6.48	6.585	−0.105	6.374	0.106	**111***	**6.97**	**7.727**	**−0.757**	**7.021**	**−0.051**
025	7.14	7.252	−0.112	7.194	−0.054	112	7.01	6.996	0.014	7.091	−0.081
026*	**7.29**	**7.962**	**−0.672**	**7.079**	**0.211**	113	7.04	7.332	−0.292	7.189	−0.149
027	5.86	6.193	−0.333	5.873	−0.013	114	7.16	7.393	−0.233	7.2	−0.04
028	8.15	8.324	−0.174	8.199	−0.049	115	7.72	7.687	0.033	7.188	0.532
029	6.64	6.463	0.177	6.31	0.33	**116***	**7.89**	**7.815**	**0.075**	**7.982**	**−0.092**
030	7.85	7.849	0.001	7.763	0.087	117	7.60	7.612	−0.012	7.676	−0.076
031*	**7.92**	**7.686**	**0.234**	**7.178**	**0.742**	118	7.46	7.705	−0.245	7.692	−0.232
032	8.00	7.981	0.019	8.195	−0.195	119	8.15	8.175	−0.025	8.362	−0.212
033	7.60	7.735	−0.135	7.948	−0.348	120	8.52	8.774	−0.254	8.429	0.091
034	7.19	7.368	−0.178	7.279	−0.089	**121***	**8.52**	**8.402**	**0.118**	**8.086**	**0.434**
035	7.42	7.324	0.096	7.404	0.016	122	8.10	8.154	−0.054	7.985	0.115
036*	**7.82**	**7.528**	**0.292**	**7.517**	**0.303**	123	7.92	8.079	−0.159	8.017	−0.097
037	7.18	7.082	0.098	7.487	−0.307	124	7.80	7.796	0.004	7.808	−0.008
038	7.42	7.277	0.143	7.16	0.26	125	7.96	8.069	−0.109	7.914	0.046
039	7.37	7.14	0.23	7.649	−0.279	**126***	**8.10**	**7.819**	**0.281**	**8.162**	**−0.062**
040	7.49	7.844	−0.354	7.782	−0.292	127	7.41	7.214	0.196	7.236	0.174
041*	**7.35**	**7.657**	**−0.307**	**7.555**	**−0.205**	128	7.62	7.658	−0.038	7.327	0.293
042	8.00	7.783	0.217	7.858	0.142	129	7.96	7.889	0.071	7.653	0.307
043	7.02	7.019	0.001	7.21	−0.19	130	8.40	8.643	−0.243	8.599	−0.199
044	7.14	7.123	0.017	7.48	−0.34	**131***	**8.40**	**9.221**	**−0.821**	**8.71**	**−0.31**
045	7.89	7.578	0.312	7.955	−0.065	132	8.70	8.576	0.124	8.432	0.268
046*	**6.95**	**7.482**	**−0.532**	**7.572**	**−0.622**	133	8.30	8.753	−0.453	8.507	−0.207
047	7.59	7.574	0.016	7.614	−0.024	134	8.70	8.414	0.286	8.022	0.678

Table 4 (continued)

No.	pIC_{50}	CoMFA		CoMSIA		No.	pIC_{50}	CoMFA		CoMSIA	
		predict	deviation	predict	deviation			predict	deviation	predict	deviation
048	7.66	7.523	0.137	7.456	0.204	135	8.40	8.686	−0.286	8.413	−0.013
049	8.00	7.844	0.156	7.782	0.218	**136***	**8.52**	**8.335**	**0.185**	**7.926**	**0.594**
050	8.15	8.142	0.008	8.115	0.035	137	8.22	8.357	−0.137	7.998	0.222
051*	**8.22**	**8.486**	**−0.266**	**8.433**	**−0.213**	138	8.15	7.88	0.27	8.127	0.023
052	7.55	7.494	0.056	7.903	−0.353	139	7.55	7.827	−0.277	7.969	−0.419
053	8.22	8.272	−0.052	8.356	−0.136	140	9.52	9.353	0.167	9.091	0.429
054	8.70	8.257	0.443	8.446	0.254	**141***	**8.70**	**8.676**	**0.024**	**8.541**	**0.159**
055	9.00	8.718	0.282	9.108	−0.108	142	8.70	8.864	−0.164	8.984	−0.284
056*	**8.52**	**8.355**	**0.165**	**8.727**	**−0.207**	143	9.00	8.659	0.341	8.933	0.067
057	8.22	8.224	−0.004	8.19	0.03	144	8.70	8.763	−0.063	8.918	−0.218
058	8.30	8.286	0.014	8.001	0.299	145	8.40	8.912	−0.512	8.515	−0.115
059	8.05	7.897	0.153	8.103	−0.053	**146***	**8.22**	**7.862**	**0.358**	**7.767**	**0.453**
060	9.00	8.367	0.633	8.302	0.698	147	8.22	8.054	0.166	8.157	0.063
061*	**5.97**	**6.442**	**−0.472**	**6.959**	**−0.989**	148	8.52	8.023	0.497	8.413	0.107
062	8.22	8.186	0.034	8.208	0.012	149	8.52	8.681	−0.161	8.651	−0.131
063	7.89	7.894	−0.004	7.899	−0.009	150	8.00	8.231	−0.231	7.781	0.219
064	7.92	8.229	−0.309	8.13	−0.21	**151***	**9.52**	**9.022**	**0.498**	**8.916**	**0.604**
065	8.05	8.074	−0.024	7.931	0.119	152	9.00	9.049	−0.049	8.958	0.042
066*	**7.20**	**8.108**	**−0.908**	**8.065**	**−0.865**	153	8.70	9.206	−0.506	8.914	−0.214
067	8.52	8.549	−0.029	8.769	−0.249	154	9.00	8.912	0.088	8.966	0.034
068	8.52	8.645	−0.125	8.724	−0.204	155	9.52	9.4	0.12	9.097	0.423
069	8.70	8.156	0.544	8.443	0.257	**156***	**9.00**	**8.724**	**0.276**	**8.517**	**0.483**
070	8.40	8.523	−0.123	8.341	0.059	157	8.22	8.168	0.052	8.323	−0.103
071*	**7.82**	**8.207**	**−0.387**	**8.111**	**−0.291**	158	9.00	9.125	−0.125	9.035	−0.035
072	8.70	8.535	0.165	8.723	−0.023	159	8.70	8.484	0.216	8.416	0.284
073*	7.96	8.031	−0.071	8.024	−0.064	160	8.70	8.707	−0.007	9.012	−0.312
074	7.77	7.874	−0.104	7.675	0.095	**161***	**7.64**	**7.761**	**−0.121**	**7.864**	**−0.224**
075	7.92	7.575	0.345	7.908	0.012	162	8.52	8.719	−0.199	8.754	−0.234
076*	**7.89**	**7.714**	**0.176**	**7.594**	**0.296**	163	8.40	8.393	0.007	8.308	0.092
077	6.58	6.81	−0.23	6.691	−0.111	164	8.40	8.482	−0.082	8.22	0.18
078	6.64	7.05	−0.41	7.112	−0.472	165	8.40	8.76	−0.36	8.528	−0.128
079	8.22	8.257	−0.037	8.278	−0.058	**166***	**8.52**	**8.911**	**−0.391**	**8.814**	**−0.294**
080	8.15	8.102	0.048	8.344	−0.194	167	8.22	8.216	0.004	8.228	−0.008
081*	**6.79**	**7.446**	**−0.656**	**6.855**	**−0.065**	168	9.52	8.848	0.672	8.923	0.597
082	8.70	8.51	0.19	8.231	0.469	169	8.10	8.372	−0.272	8.245	−0.145
083	8.15	8.272	−0.122	8.243	−0.093	170	8.10	8.013	0.087	8.136	−0.036
084	9.00	9.191	−0.191	8.918	0.082	**171***	**9.00**	**8.396**	**0.604**	**8.891**	**0.109**
085	8.70	8.724	−0.024	8.868	−0.168	172	8.52	8.591	−0.071	8.408	0.112
086*	**7.82**	**8.579**	**−0.759**	**8.138**	**−0.318**	173	9.00	8.965	0.035	8.974	0.026
087	8.15	7.768	0.382	7.833	0.317	**174***	**9.00**	**8.489**	**0.511**	**9.049**	**−0.049**

*molecules belonged to the test set

analysis used the five force fields. The contributions of steric, electrostatic, hydrophobic, hydrogen-bond donor field, and hydrogen bond acceptor field are 9.8%, 35.1%, 22.9%, 17.1%, and 15.2% respectively. As the results show, the electrostatic, hydrophobic and hydrogen-bond effect (including hydrogen-bond donor field and hydrogen bond acceptor field) were the main factors affecting the binding inhibitory activity. We derived a model with a high q^2 value of 0.520 and a conventional r^2 value of 0.872 for five components. The predicted versus experimental activities were

Table 5 Statistical parameters of CoMFA and CoMSIA models of the training sets based on docking analysis

	NOC	q^2	r^2	SD	F	Fraction of field contribution				
						S	E	H	D	A
CoMFA	5	0.501	0.887	0.225	206.225	0.446	0.554			
CoMSIA	5	0.520	0.872	0.239	180.443	0.098	0.351	0.229	0.171	0.152

S-steric; E-electrostatic; D-donor; A-acceptor; H-hydrophobic; q^2 -LOO of cross-validated correlation coefficient; r^2 -non-cross-validated correlation coefficient; SD-predicted standard deviation; *F*-*F* test values; NOC-number of optimum component

displayed in Fig. 9A and 9B. As was shown, most of the molecules were drawn on or near the diagonal line, which indicated that the predicted pIC_{50} value models were in good agreement with the actual data, manifesting the rational and potent fitting power and the convincing predictive ability.

To validate the 3D-QSAR models, 34 inhibitors (*-denoted in Table 4) which were not included in forming CoMFA and CoMSIA models, were selected as testing compounds. The results were also shown in Table 5 (● labeled). The deviations of the predicted pIC50 values from the corresponding experimental pIC50 values were always lower than 1.0 log unit in both models. To explain the structural differences of binding modes between the training set and the test set of compounds, automated molecular docking was conducted for the test set by the same method as that of the training set. The testing results for the 34 inhibitors indicated that the CoMFA and CoMSIA models could be able to apply to new molecules designed for Chk1.

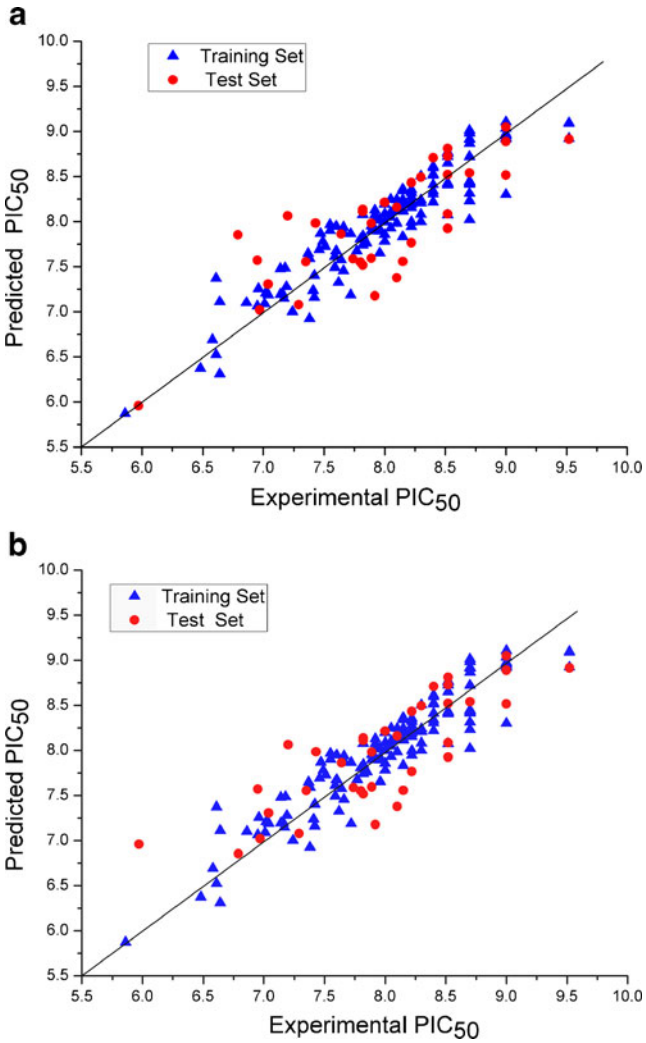

Fig. 9 CoMFA and CoMSIA models of activity (pIC_{50}) predicted values and experimental values. "▲" on behalf of the training set, "●" on behalf of test set

Mapping of CoMFA and CoMSIA model into Chk1 binding site

The fields based on ligands may not be enough to explain the interactions between the inhibitors and the receptor. Therefore, more information for modification of the reported inhibitors and the results of the docking studies could be acquired, which could be complements of 3D-QSAR studies for drug design. Based on the alignments of the binding conformations, the CoMFA analyses of steric and electrostatic fields were presented as contour plots in Fig. 9. Compound 155 was shown in the maps to contribute to visualization. There were two large green contour regions around 3- and 6'-position, where bulky substituents significantly would increase the biological activities (Fig. 10A). Because these positions were at the entrance of the active site in the structure of receptor binding pocket, bulky substituents were allowed in these areas. Moreover, one yellow polyhedron near 4-position and the other yellow region around GLU91 may suggest that in these positions decreased bulky substituents would improve biological activities. According to the environment surrounding the binding sites, the bulk of substituents were limited by GLY89, GLY 90, GLU91 and ASP94 in these regions. Therefore, bulky substituents are unfavorable to the biological activities.

In the CoMFA electrostatic contour maps (Fig. 10B), there were blue areas around 3 - position and 4 - position where positively charged groups may help to improve the activity. According to the environment in binding site, the 4-position adjoins the ASP94 which was negatively charged amino acids. Therefore, positively charged substituent (compare 70 and 71 with 78 and 81) were beneficial to the

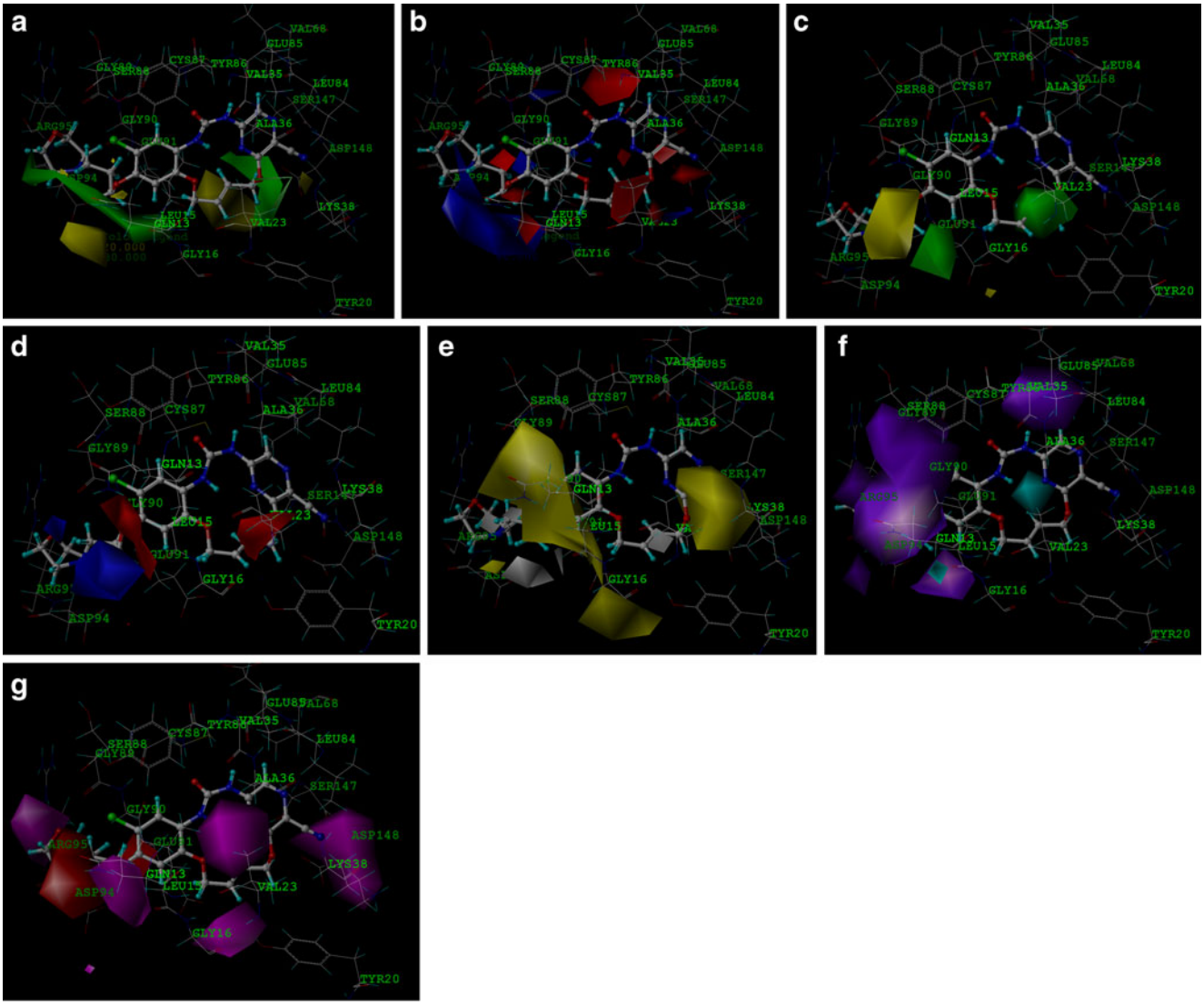

Fig. 10 (**A**) CoMFA steric field contour maps (green: favored; yellow, disfavored); (**B**) CoMFA electrostatic field contour maps (red: disfavored areas of positive potential, blue: favored areas of positive potential); (**C**) CoMSIA steric field contour maps (green: favored; yellow, disfavored); (**D**) CoMSIA electrostatic field contour maps (red: disfavored areas of positive potential, blue: favored areas of positive potential); (**E**) CoMSIA hydrophobic field contour maps (yellow: favored, white regions disfavored); (**F**) CoMSIA H-bond donor(cyan: favored, purple: disfavored); (**G**) CoMSIA H -acceptor field contour maps (magenta: favored, red: disfavored). The maps generated depict regions having scaled coefficients greater than 80% (favored) or less than 20% (disfavored). Compound 155 was superposed as the reference molecules in the maps

activity in these positions. Besides, there were red regions near 4,8- position and on either side of the 5′, 6-position. Increasing the electronegativity of substituents in these positions may improve the activity due to the amino acid residues around these regions. For example, LEU15 near the 4-position, TYR86 around the 8-position, VAL23, SER147 and ASP148 on both sides of 5′, 6-position, all these amino acid residues had positive charges, consequently, electronegative substituents were favorable to enhance the activity in these positions.

The results of steric and electrostatic regions of CoMSIA were shown in Fig. 10C and Fig. 10D. Compared with the result of CoMFA, there was not much difference between them. As shown in Fig. 10C and Fig. 10D, small substituents were favorable for antagonist activity near the 4- position; while introducing bulky substituent into the region around 3, 6'- position would increase the antagonist activity. In addition, electropositive substituents were favorable for antagonist activity in 4-position, yet strong electronegative substituent may enhance the antagonist activity around the 6'-position. For example, the activities of compound 158, 159 and 160 with N atom in the 4-position were better than the activities of compound 91, 92 and 93 with C atom in the 4-position.

The CoMSIA contour plots expressed yellow-colored regions, where increased hydrophobic interaction was related to enhance biological activities. While in white-colored regions decreased hydrophilic interaction was associated with increased biological activities. As shown in Fig. 10E, the big yellow polyhedrons between 3, 4 - position indicated a hydrophobic group substitution was favored at these sites. Hydrophobic tank was formatted by GLY89, GLY 90 and GLN13, LEU15 amino acids around 3, 4 –position. The white areas surrounding the group in the 6′-position and the side chain of substituent in the 4-position may indicate that any hydrophilic group substitution would be preferred at this site. According to the environment in binding site, the side chain of substituent in the 4-position was close to the entrance of the active site. Besides, the hydrophilic amino acid ARG95 was around the white area.

The cyan and purple regions indicated that hydrogen-bond donor substituents were favorable and unfavorable for antagonist activity. The regions where hydrogen-bond acceptor substituents were favorable or unfavorable for antagonist activity indicated in magenta or red. As Fig. 10F shows, due to hydrogen bonding between the amino acid

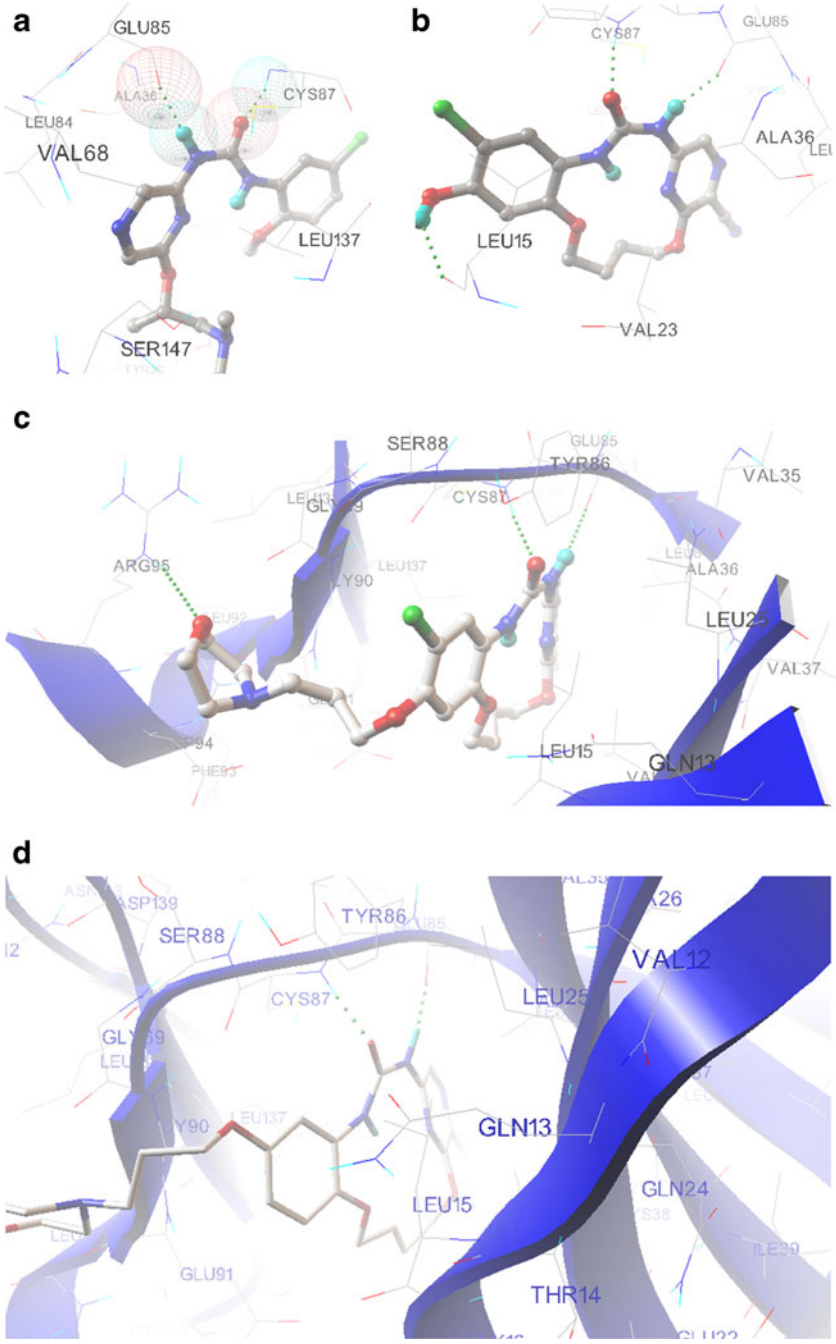

Fig. 11 Data set compounds docked conformation and the binding pocket amino acids form hydrogen bonds (green dotted line below)

residues (TYR86 and CYS87) and the group of hydrogen-bond donor in 9-position, a region of cyan contour near the 9-position indicated that hydrogen-bond donor substituents may increase the antagonist activity. And there was a cyan contour region near the carbonyl group of the amino acid residues (LEU15 and GlY16), where hydrogen-bond donor substituents may enhance the antagonist activity. While several purple contour areas between GLU91 and GLY16, near GLN13, TYR86 and GLY89 may suggest that hydrogen-bond donor substituents may decrease the antagonist activity. In addition, as Fig. 10G shows, two red contour regions around the side chain of substituent in the 4-position indicated that hydrogen-bond acceptor substituents would decrease the biological activities in the region. While several magenta contour areas around the amino acid residue ARG95, LEU15, TYR20, VAL23, LYS38 and ASP148 indicate that hydrogen-bond acceptor substituents were favorable for the antagonist activity in the 1'-,5'-,7'- 3-position and the side chain of substituent in the 4-position.

Figure 11 displayed the hydrogen bonding interaction between inhibitors and amino acid residues. The carbonyl of GLU85 formed a H-bond contact with the H atom in the 7-position; the 8-carbonyl group was hydrogen-bonded to the CYS87 NH group; 9-hydroxyl group in the 4-position formed a H-bond with the carbonyl of LEU15; and the O atom in the substituent group of 4-position accepted a H-bond from the amide group of ARG95. Furthermore all the angles of hydrogen bonding were greater than 150 degrees, and all the distances of hydrogen bonding were less than 3 Å.

To sum up, small bulk, positively charged, hydrogen bond acceptor and hydrophilic groups are favored around 4-position. While bulky, electronegative, hydrophobic groups can enhance the activity around 3, 6'- substituted. In addition, in the docking process, the data set molecules and the amino acid residues in the binding pocket can form hydrogen bonding, which involves the O atom in 8-position, the H atom of NH in 9-position, and the polar substituent groups in 4-position.

Conclusions

In this study, 3D-QSAR studies and molecular docking were carried out, not only to illustrate the interaction mechanism between CHK1 receptor and 174 inhibitors, but also to build highly accurate and predictive 3D-QSAR models, including the CoMFA (r^2, 0.501; q^2, 0.887) and CoMSIA (r^2, 0.520; q^2, 0.872) models based on flexible docking alignment to predict the biological activity of new compounds. Besides, the particular structures of CHk1 binding with the compounds were shown by molecular docking. Further, in this paper visualization of the 3D-QSAR model of the molecules under study offered details of the relationship between structure and activity, and thus would provide explicit indications for the design of better analogues.

Acknowledgments The authors gratefully acknowledged financial support from the Natural Science Foundation of China (NO. 21071021).

References

1. Chen Y, Sanchez Y (2004) Chk1 in the DNA damage response: conserved roles from yeasts to mammals. DNA Repair 3:1025–1032
2. Kastan MB, Onyekwere O, Sidransky D et al (1991) Participation of p53 protein in the cellular response to DNA damage. Cancer Res 51:6304–6311
3. Li Q, Zhu GD (2002) Targeting serine/threonine protein kinase B/Akt and cell-cycle checkpoint kinases for treating cancer. Curr Top Med Chem 2:939–971
4. Greenblatt MS, Bennett WP, Hollstein M et al (1994) Mutations in the p53 tumor suppressor gene: clues to cancer etiology and molecular pathogenesis. Cancer Res 54:4855–4878
5. Yolanda S, Calvin W, Richard ST et al (1997) Conservation of the chk1 checkpoint pathway in mammals: linkage of DNA damage to cdk regulation through Cdc25. Science 277:1497–1501
6. Cramer RD, Patterson DE, Bunce JD (1988) Comparative molecular field analysis (CoMFA). 1. Effect of shape on binding of steroids to carrier proteins. J Am Chem Soc 110:5959–5967
7. Cramer RD, Bunce JD, Patterson DE et al (1988) Crossvalidation, bootstrapping, and partial least squares compared with multiple regression in conventional QSAR studies. Quant Struct Act Relat 7:18–25
8. Klebe G, Abraham U, Mietzner T (1994) Molecular similarity indices in a comparative analysis (CoMSIA) of drug molecules to correlate and predict their biological activity. J Med Chem 37:4130–4146
9. Potashman MH, Bready J, Coxon A et al (2007) Design, synthesis, and evaluation of orally active benzimidazoles and benzoxazoles as vascular endothelial growth factor-2 receptor tyrosine kinase inhibitors. J Med Chem 50:4351–4373
10. Yang GF, Lu HT, Xiong Y et al (2006) Understanding the structure activity and structure-selectivity correlation of cyclic guanine derivatives as phosphodiesterase-5 inhibitors by molecular docking, CoMFA and CoMSIA analyses. Bioorg Med Chem 14:1462–1473
11. Huang X, Xu L, Luo X et al (2002) Elucidating the inhibiting mode of AHPBA derivatives against HIV-1 protease and building predictive 3D-QSAR models. J Med Chem 45:333–343
12. Li GQ, Tao ZF, Tong YS (2007) Synthesis and in-vitro biological activity of macro cyclic urea Chk1 inhibitors. Bioorg Med Chem Lett 17:6499–6504
13. Wang GT, Li GQ (2005) 1-(5-Chloro-2-alkoxyphenyl)-3-(5-cyano-pyrazi-2-yl)ureas as potent and selective inhibitors of Chk1 kinase: synthesis, preliminary SAR, and biological activities. J Med Chem 48:3118–3121
14. Li GQ, Hasvold LA, Tao ZF (2006) Synthesis and biological evaluation of 1-(2,4,5-trisubstituted phenyl)-3-(5-cyanopyrazin-2-yl)ureas as potent Chk1 kinase inhibitors. Bioorg Med Chem Lett 16:2293–2298
15. Tao ZF, Wang L, Stewart KD et al (2007) Structure-based design, synthesis, and biological evaluation of potent and selective macrocyclic checkpoint kinase 1 inhibitors. J Med Chem 50:1514–1527
16. Tao ZF, Chen ZH (2007) Macrocyclic ureas as potent and selective Chk1 inhibitors: an improved synthesis, kinome profiling,

structure–activity relationships, and preliminary pharmacokinetics. Bioorg Med Chem Lett 17:6593–6601
17. Li GQ, Tao ZF, Tong YS (2007) Synthesis and in-vitro biological activity of macrocyclic urea Chk1 inhibitors. Bioorg Med Chem Lett 17:6499–6504
18. Tao ZF, Wang L, Stewart KD et al (2007) Structure-based design, synthesis, and biological evaluation of potent and selective macrocyclic checkpoint kinase 1 inhibitors. J Med Chem 50:1514–1527
19. Sybyl Version 7.0 (2004) St. Louis (MO), Tripos Associates Inc. http://www.tripos.com
20. Clark M, Cramer RD III, Opdenbosch NV (1989) Validation of the general purpose tripos 5.2 force field. J Comput Chem 10:982–1012
21. Gasteiger J, Marsili M (1980) Iterative partial equalization of orbital electronegativity- a rapid access to atomic charges. Tetrahedron 36:3219–3228
22. Morris GM, Goodsell DS, Halliday RS et al (1998) Automated docking using a Lamarckian generic algorithm and empirical binding free energy function. J Comput Chem 19:1639–1662
23. Weiner SJ, Kollman PA, Case DA et al (1984) A new force field for molecular mechanical simulation of nucleic acidsand proteins. J Am Chem Soc 106:765–784
24. Gasteiger J, Marsili M (1980) Iterative partial equalization of orbital electronegativity– a rapid access to atomic charges. Tetrahedron 36:3219–3228
25. Mehler EL, Solmajer T (1991) Electrostatic effects in proteins: comparison of dielectric and charge models. Protein Eng 4:903–910
26. Bush BL, Nachbar RB (1993) Sample-distance partial least squares: PLS optimized for many variables, with application to CoMFA. J Comput Aided Mol Des 7:587–619